Enhanced doping effects of multielement on anisotropic thermal expansion in ZrO$_2$ with new compositions

Liu Qu[a], Kwang-Leong Choy[a,*], Richard Wheatley[b]

[a] UCL Institute for Materials Discovery, University College London, London, WC1E 6BT, UK
[b] Department of Chemistry, University of Nottingham, Nottingham, NG7 2RD, UK
* Corresponding Author: Tel/fax: +44(0)2076793855.
E-mail address: k.choy@ucl.ac.uk (K.-L. Choy)

Abstract

Coefficient of thermal expansion (CTE) of a solid material plays a critical role for a variety of high temperature applications such as thermal barrier coating (TBC) systems during the thermal cycling process. Ceramics contain ionic bonds; hence they tend to exhibit lower CTE values than alloys/metals. Developing new ceramic thermal barrier materials using promising dopants and compositions that have higher CTE values than the conventional 6-8 wt.% Y$_2$O$_3$ stabilized ZrO$_2$ (8YSZ) will contribute to the decrease in thermal expansion mismatch between a typical ceramic 8YSZ (10~11×10^{-6} °C^{-1}) top coat and a metal alloy based bond coat such as NiCrAlY (14~17×10^{-6} °C^{-1}),[1, 2] which is highly desirable. This work reports design, modelling, synthesis, and characterization of promising new compositions based on Dy^{3+}, Al^{3+} and Ce^{4+} doped YSZ that consist of the tetragonal structure and have an enhanced thermal expansion than 8YSZ. The intrinsic CTE at the atomic level has been investigated via molecular dynamics (MD) simulation. The atomic scale analysis provides new insights into the enhanced doping effects of multiple trivalent and tetravalent cations on the lattice structure, lattice energy and thermal expansion in ZrO$_2$. The calculated lattice energy becomes smaller with the incorporation of Dy^{3+}, Al^{3+}, and Ce^{4+} ions, which corresponds strongly to the increase in CTE. The crystalline size is reduced due to the incorporation of the Al^{3+} and Ce^{4+}, whereas the sintering resistance is enhanced ascribed to the addition of Dy^{3+} and Al^{3+}. Doping Dy^{3+}, Al^{3+},

and Ce^{4+} cations to YSZ increased the CTE value of YSZ and for $Dy_{0.03}Y_{0.075}Zr_{0.895}O_{1.948}$, the CTE is 12.494×10^{-6} °C^{-1} at 900°C, which has an 11% increase, as compared with that of 8YSZ.

Keywords: Coefficient of thermal expansion; lattice structure; molecular dynamics simulation; new thermal barrier materials;

Introduction

Structural oxide materials such as Y_2O_3 partially stabilized ZrO_2 (YSZ) have physical, thermomechanical and electrochemical properties that are desirable in high-temperature applications such as gas turbines, solid oxide fuel cells, gas sensors, and so forth.[2-4] YSZ has a relatively low density of 6.4 g.cm^{-3} and its hardness is 14 GPa, contributing to high erosion resistance and low parasitic forces on turbine blades.[2] The melting point of YSZ is reported to be 2700°C and the tetragonal structure can be maintained up to 2370°C.[5, 6] Oxygen vacancy concentration in the lattice of YSZ modifies the atomic structure, hence impacting chemical, physical and mechanical properties. For instance, the presence of oxygen vacancies in YSZ contributes to the weakening of the ionic bond, induces a phase transformation from tetragonal structure to cubic structure, and enhances the anion conductivity at high temperatures.[7] The adsorption and dissociation of oxygen on YSZ surfaces contribute to the formation of O^- and O_2^- that show catalytic activity in terms of oxidizing hydrocarbons.[8] It is reported that cubic YSZ has a lower fracture toughness (6 J.m^{-2}) than tetragonal YSZ (45-150 J.m^{-2}), thus leading to a poor thermal cycling life.[9]

In particular, one of the critical material properties of YSZ is high CTE for TBC materials. The CTE of conventional TBC materials (6-8 wt.% YSZ) is $10 \sim 11 \times 10^{-6}$ °C^{-1}, whereas the underlying bond coat such as NiCrAlY has a higher CTE ($14 \sim 17 \times 10^{-6}$ °C^{-1}).[1, 2] During the thermal cycling process at a high temperature (e.g. 1250°C), the thermal expansion mismatch generates thermal stress and decreases the durability of TBCs. The thermal expansion of TBCs needs to be improved to match that of the metallic substrate and bond coat in order to reduce

2

the thermal stress and to increase the thermal cyclic life.[10] Thermal expansion is a result of anharmonic terms from the potential energy, higher than the quadratic terms.[11, 12] When 2%-6% Dy^{3+} and 5% Ce^{4+} were added to YSZ, the CTE values were reported to be increased, whereas the higher doping contents of Dy^{3+} to YSZ can decrease the CTE and reduce the thermochemical stability.[13, 14] However, atomic scale insights into the doping effects of trivalent and tetravalent cations on lattice structure, lattice energy and thermal expansion in ZrO_2 have yet to be comprehensively established and reported. Al^{3+} is one of the smallest trivalent metal cation, and Dy^{3+} has a larger ionic radius and smaller bonding energy than Zr^{4+} (Table 1),[15] which could potentially enhance the thermal expansion coefficient of YSZ. CeO_2 is a promising dopant for YSZ due to its potential capability to increase tetragonal phase stability,[16] resistance to hot corrosion[17] and thermal cycling behaviour of YSZ.[18] Dy^{3+}, Al^{3+} and Ce^{4+} cations were selected to dope YSZ because of their unique valence, weight, ionic radius, and bonding energy that are vital factors in controlling the ion vibration in the lattice and thermal expansion of YSZ.[19]

	Dy^{3+}	Al^{3+}	Ce^{4+}	Zr^{4+}	Y^{3+}
Ionic radius (Å)	1.03	0.54	0.97	0.84	1.02
Bonding energy (kJ·mol^{-1})	615	501.9	790	766.1	714.1
Atomic weight (g·mol^{-1})	162.5	26.982	140.116	91.224	88.906

Table 1. Ionic radius (CN=8 for Dy^{3+}, Ce^{4+}, Zr^{4+} and Y^{3+}, CN=6 for Al^{3+}) and bonding energy for the selected cations, adapted from [15].

The novel aspect of this study is to: (a) use MD simulation to gain insights into enhanced doping effects of multiple trivalent and tetravalent cations on the lattice structure and thermal expansion in ZrO_2 to facilitate the development of new thermal barrier materials; and (b) conduct the experimental validation of the new thermal barrier materials by synthesizing the new compositions of Dy^{3+}, Al^{3+} and Ce^{4+} doped YSZ using the sol-gel method in order to achieve good stoichiometry control, and investigate their lattice structure and CTEs. Combinations of trivalent and tetravalent cations with various ionic radius and bonding energy

have been selected and incorporated to ZrO_2 to comprehensively understand their effects on CTEs, lattice structure and lattice energy. The fabricated Dy^{3+}, Al^{3+} and Ce^{4+} doped YSZ have been characterized using a combination of X-ray diffraction (XRD) and Raman spectroscopy. The CTE of the bulk samples is measured up to 1000°C. MD simulation is effective in terms of calculating the dynamic properties of Dy^{3+}, Al^{3+} and Ce^{4+} doped YSZ based on Newton's second law of motion.[20] It enables the intrinsic transport properties which are sensitive to microstructural features to be calculated without the influence of lattice imperfections.[21, 22] Theoretical material properties including the lattice energy and anisotropic CTE are calculated by MD simulation, with an in-depth understanding on the effects of doping on lattice structure and thermal expansion in ZrO_2 that would greatly facilitate the materials design.

Computational Details

MD simulation was performed to calculate the lattice energy and CTE. A rigid ion model with $6\times6\times32$ simulation cells of a tetragonal lattice was utilized to describe the simulation system. The simulation box consisted of 2304 cation sites, which were fully filled or had one random vacancy, and 4608 anion sites, which included a number of random vacancies. Lattice constants were measured by XRD using a Siemens D500 X-ray diffractometer (Cu-Kα radiation, λ=1.54 Å) and DIFFRAC^{plus} software was applied to processing the diffraction data. The measured lattice constants were used as the starting parameters and input into the simulation for the calculation. The potential, V_{ij}, was calculated using the Buckingham potential for the short-range interaction between ions and a long-range Coulomb interaction,

$$V_{ij} = A_{ij} \exp\left(\frac{-r_{ij}}{\rho_{ij}}\right) - \frac{C_{ij}}{r_{ij}^6} + \frac{Q_i Q_j}{4\pi\varepsilon_0 r_{ij}}, \tag{1}$$

where A_{ij}, ρ_{ij} and C_{ij} are Buckingham potential parameters, Q_i, Q_j and r_{ij} describe the Coulomb interaction where Q_i and Q_j are the charges of two ions, r_{ij} is the separation of two ions, and ε_0 is the vacuum permittivity.[23, 24] All simulations were carried out at 0 bar and in an isothermal

bath at temperatures between 295 K and 1873 K. The potential parameters are presented in Table 2. Cation-cation short-range interaction parameters were set to zero.

Species	A (eV)	ρ (Å)	C (eV·Å^6)	Ref.
Zr^{4+}-O^{2-}	1502.11	0.345	5.1	[23]
Y^{3+}-O^{2-}	1366.35	0.348	19.6	[23]
Dy^{3+}-O^{2-}	1807.84	0.3393	18.77	[25]
Al^{3+}-O^{2-}	1142.6775	0.2991	0	[26]
Ce^{4+}-O^{2-}	1986.8	0.3511	20.4	[27]
O^{2-}-O^{2-}	9547.96	0.224	32	[23]

Table 2. Buckingham potential parameters of Dy^{3+}, Al^{3+} and Ce^{4+} doped YSZ.

The charges were -2e for O atoms, +4e for Zr and Ce atoms, and +3e for Dy, Al, and Y atoms. Dy^{3+}, Al^{3+}, Y^{3+}, Zr^{4+} and Ce^{4+} were randomly distributed in the cation sites, while O^{2-} ions were randomly located in the anion sites. Short-range forces were calculated using a direct summation in which a cut-off radius was applied, and a long-range correction was added. The long-range forces were determined using the Wolf method.[28, 29] The temperature in the (N, P, T)-ensemble was adjusted using the Berendsen barostat method and the pressure was controlled using the Anderson thermostat method.[30, 31] In the (N, P, T)-ensemble, the atoms were equilibrated at each temperature. The (N, P, T)-ensemble consisted of 1×10^5 MD steps (50 ps) which included 5×10^4 equilibration steps (25 ps). Based on the simulation, the equilibrated lattice constant and the lattice energy were computed. A nonlinear regression equation with forth order polynomial [Supporting Information, Equation (2)-(9)] was fitted to the lattice constant data to calculate the theoretical CTE from equation 2,

$$\alpha = \frac{1}{L_0} \cdot \frac{dL}{dT},$$ (2)

where α is the thermal expansion coefficient, L_0 is the lattice constant at original temperature and $\frac{dL}{dT}$ is the lattice constant change against temperature.[32] $\frac{dL}{dT}$ was calculated by the first

derivative of the nonlinear regression equation and L_0 was the initial equilibrated lattice constant (Table S1-S4).

Experimental Details

Samples of Dy^{3+}, Al^{3+} and Ce^{4+} doped YSZ and 8YSZ were synthesized using a sol-gel route to facilitate the precise control of the stoichiometry of the multicomponent oxides. Initially, metal salts and acetylacetone (AcAc) were dissolved in 1-propanol by vigorous stirring, with the desired molar ratio under Ar atmosphere. Zirconium propoxide [$Zr(OPr)_4$] in 1-propanol were added to the solution of metal salts and AcAc in 1-propanol was added to the metal salts solution. Deionized water was added to the 1-propanol, the solution was subsequently mixed with the $Zr(OPr)_4$ solution. This solution was mechanically stirred for 30 minutes and was heated at 50°C to form a gel. The gel was dried at 120°C, followed by a 3-hour calcination at 950°C in air to form oxide powders. Dy^{3+}, Al^{3+} and Ce^{4+} doped YSZ and 8YSZ powders were sintered at 1200°C for 2 hours, subsequently compacted into bulk pellets and sintered at 1200°C for 6 hours. The typical thickness of samples was within the range of 2.27 - 4.20 mm with a diameter of 5.00 mm.

The crystal structure was characterized by XRD using a Siemens D500 X-ray diffractometer (Cu-Kα radiation, λ=1.54 Å). Raman analysis was conducted using a Horiba Jobin-Yvon LabRAM spectrometer equipped with an Olympus BX41 microscope (He-Ne laser source, 632.8 nm) and a Renishaw inVia Raman microscope equipped with an Ar ion laser at a wavelength of 514.5 nm. The CTEs were measured using a NETZSCH DIL 402C dilatometer from room temperature to 1000°C with a heating rate of 5°C.min^{-1} in air.

Results and Discussion

Modelling and Materials Design

In order to select the relevant cations to be doped into YSZ and the synergistic impact of doping multivalent cations into YSZ on the intrinsic and anisotropic thermal expansion, MD

simulation was utilised for the computation of lattice structure and energy changes at the atomic scale. The lattice constant predicted by the simulation at 1073 K is presented in Table 3. The lattice constant increased due to doping with larger cations such as Dy^{3+} and Ce^{4+}, whereas it decreased because of doping with smaller cation such as Al^{3+} to 3Dy-YSZ.

	8YSZ	$Dy_{0.03}Y_{0.075}Zr_{0.895}O_{1.948}$	$Dy_{0.03}Al_{0.03}Y_{0.081}Zr_{0.859}O_{1.929}$	$Dy_{0.03}Ce_{0.05}Y_{0.080}Zr_{0.84}O_{1.945}$
$a=b$ (Å)	3.6361	3.6420	3.6377	3.6577
c (Å)	5.1429	5.1520	5.1445	5.1726

Table 3. Predicted lattice constants of multicomponent oxides at 1073 K.

In the tetragonal lattice, each cation is coordinated with 8 anions in a distorted cubic block (Figure 1). The bond length of Zr^{4+}-O^{2-} and Zr^{4+}-Zr^{4+} was calculated using VESTA software based on the predicted lattice constants from the MD simulation and is presented in Figure 2. The bond length increased with the addition of 3% Dy^{3+} and 5% Ce^{4+} to 8YSZ, whereas the incorporation of 3% Al^{3+} to 3Dy-YSZ decreased the bond length.
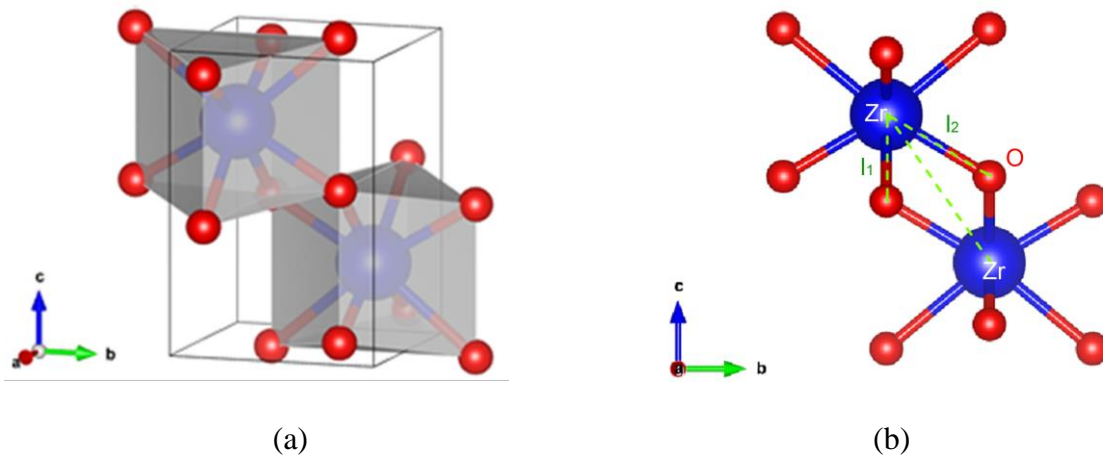

(a)   (b)

Figure 1. Lattice structure of a tetragonal ZrO_2 (*P4₂/nmc*, Zr^{4+} is in blue and O^{2-} is in red): (a) 3D view; and (b) along the a-axis.
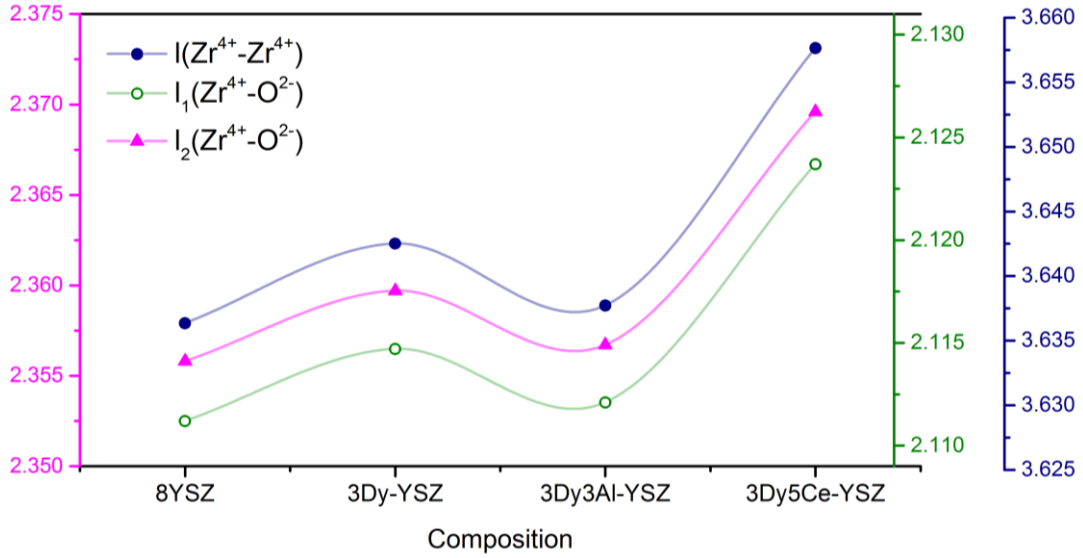
Figure 2. Distance between Zr^{4+} and Zr^{4+} and bond length of Zr^{4+}-O^{2-} at 1073 K (units: Å).

The predicted lattice energy (U) at 1073 K is shown in Table 4. The lattice energy becomes smaller because of the incorporation of Dy^{3+}, Al^{3+} and Ce^{4+} cations to 8YSZ. As the CTE increases with the decrease in the lattice energy,[33] the addition of Dy^{3+}, Al^{3+} and Ce^{4+} cations could potentially contribute to the increase in CTE values.

	8YSZ	$Dy_{0.03}Y_{0.075}Zr_{0.895}O_{1.948}$	$Dy_{0.03}Al_{0.03}Y_{0.081}Zr_{0.859}O_{1.929}$	$Dy_{0.03}Ce_{0.05}Y_{0.080}Zr_{0.84}O_{1.945}$
U (eV)	107.77	106.54	105.34	105.95

Table 4. Predicted lattice energy of various rare earth cations doped zirconia at 1073 K.

The CTE of a tetragonal oxide is anisotropic with respect to *a*-, *b*- and *c*- crystallographic axes in a unit cell. The predicted lattice constant against temperature was fitted to the nonlinear regression equation in each axis [Supporting Information, Equation (2)-(9)], and the thermal expansion was calculated from $\frac{1}{L_0} \cdot \frac{dL}{dT}$.[32] The experimental CTE was determined using NETSCH Proteus® software with a temperature difference of 100 K, and this does not qualitatively affect the comparison. In the MD simulation, the incorporation of Dy^{3+}, Al^{3+} and Ce^{4+} cations to 8YSZ has led to the increase in the CTE along the *a*- and *b*- axes, whereas predicted CTE along the *c*- axis shows a decreasing trend due to Dy^{3+}, Al^{3+} and Ce^{4+}

8

substitution. The predicted average CTE values of Dy^{3+}, Al^{3+} and Ce^{4+} incorporation to YSZ are higher than that of YSZ, in a similar trend with experimental results. Measured and calculated CTE data at 1073 K is displayed in Table 5.

	8YSZ	$Dy_{0.03}Y_{0.075}Zr_{0.895}O_{1.948}$	$Dy_{0.03}Al_{0.03}Y_{0.081}Zr_{0.859}O_{1.929}$	$Dy_{0.03}Ce_{0.05}Y_{0.080}Zr_{0.84}O_{1.945}$
CTE (*a*-/*b*-)	3.6532	8.1313	5.5116	6.7527
CTE (*c*-)	7.2237	6.9274	6.2273	7.0460
Average CTE	4.8434	7.7300	5.7501	6.8505
Tetragonality $(\frac{c}{\sqrt{2}a})$	1.0001	1.0003	1.0000	1.0000
CTE via experiment	11.1214	12.1179	11.9893	12.0921

Table 5. CTEs of various cations doped zirconia as determined via MD simulation and experiment at 1073 K (CTE units: $10^{-6} \cdot K^{-1}$).

Anisotropic thermal expansion along the *a-*, *b-* and *c-* axes of non-cubic crystalline solids such as tetragonal structure, results from the elastic anisotropy.[34] In anisotropic crystalline solids, the volumetric CTE (α_v) can be calculated from the linear CTEs of the *a-/b-* and *c-* axes by,

$$\alpha_v = 2\alpha_{a/b} + \alpha_c \tag{3}$$

where $\alpha_{a/b}$ and α_c are CTEs along *a-/b-* direction and *c-* direction, respectively.[35] In a cubic crystalline solid, the linear CTE is derived from the volumetric CTE by $\alpha_l = \frac{1}{3}\alpha_v$. Measured thermal expansion by $\frac{d(\frac{\Delta L}{L_0})}{dT}$ corresponds to an average of linear CTEs over *a-*, *b-*, and *c-* axes, due to isotropic crystalline phases in the longitudinal direction of a sample.

A Grüneisen model has been proposed for the computation of thermal expansion (α_v) for the isotropic system via,

$$\alpha_v = \frac{\gamma C_v}{k_0 V_m}, \tag{4}$$

9

where γ is Grüneisen parameter, k_0 is the bulk modulus, V_m is the molar volume and C_v is the isochoric specific heat per mole.[36] The compositional dependence of isotropic CTEs of YSZ on the Y^{3+} concentration has been investigated using a MD simulation based on the Grüneisen model.[37] The calculated CTEs were approximately 20% smaller, as compared with the measured value, whereas the addition of Y^{3+} to ZrO_2 lattice resulted in an increase in the bulk modulus and a decrease in CTEs.

Furthermore, the addition of Dy^{3+} to YSZ decreases the anisotropy of CTE (α_c/α_a),[38] whereas adding Al^{3+} and Ce^{4+} to YSZ leads to an increase in CTE anisotropy. Al^{3+} has a smaller ionic radius and atomic weight, while Ce^{4+} has a larger ionic radius and atomic weight, as compared with Zr^{4+}, which enhances the anharmonic interaction of ions. Dynamic variation of the tetragonality ($c/\sqrt{2}a$ ratio) has been calculated to assess phase stability at elevated temperatures. Doping Dy^{3+} to YSZ enhances the tetragonality, whereas doping Al^{3+} and Ce^{4+} to YSZ leads to a slight reduction in the tetragonality at 1073 K. The t'- ($1.000<c/\sqrt{2}a<1.010$) and t''- ($c/\sqrt{2}a=1.000$) tetragonal structures have been reported to be metastable phases with increased resistance to phase transformation and high mechanical properties.[39] Hence, the addition of Dy^{3+}, Al^{3+} and Ce^{4+} to YSZ facilitates the formation of the desirable t'- /t''- tetragonal structure. From the simulation, different doping of multi-cation and their concentrations as well as the resultant stoichiometries of multi-cation doped YSZ have been established, as shown in Table 5, and this has guided the materials design of multi-cation doped YSZ and validated experimentally.

Structural Characterization

The crystal structure of doped YSZ was characterized by XRD and the results are shown in Figure 3. The main phase composition has a tetragonal structure and no diffraction peaks from other phases are identified. Additionally, the double-peak (004) and (220) in the XRD in Figure 4 were obtained using a slow-scan process. The addition of Dy^{3+} to YSZ slightly decreased the

differences of the 2θ angles for (004) and (220), whereas doping Ce^{4+} resulted in the decrease of (004) and (220) with a separation of 0.6792°. When Zr^{4+} is substituted by Dy^{3+} and Al^{3+} cations, oxygen vacancies would form, bringing about the tetragonal distortion of the oxygen sublattice. In contrast, doping Ce^{4+} to YSZ would create less oxygen-sublattice distortion because less oxygen vacancy can be formed in Ce^{4+} substituting Zr^{4+} than in Dy^{3+} substituting Zr^{4+}.[40] The ionic radius of Al^{3+} (0.54 Å) is smaller than that of Ce^{4+} (0.97 Å),[15] suggesting that the lattice distortion due to the Al^{3+} incorporation would be larger than that resulting from the Ce^{4+} incorporation.
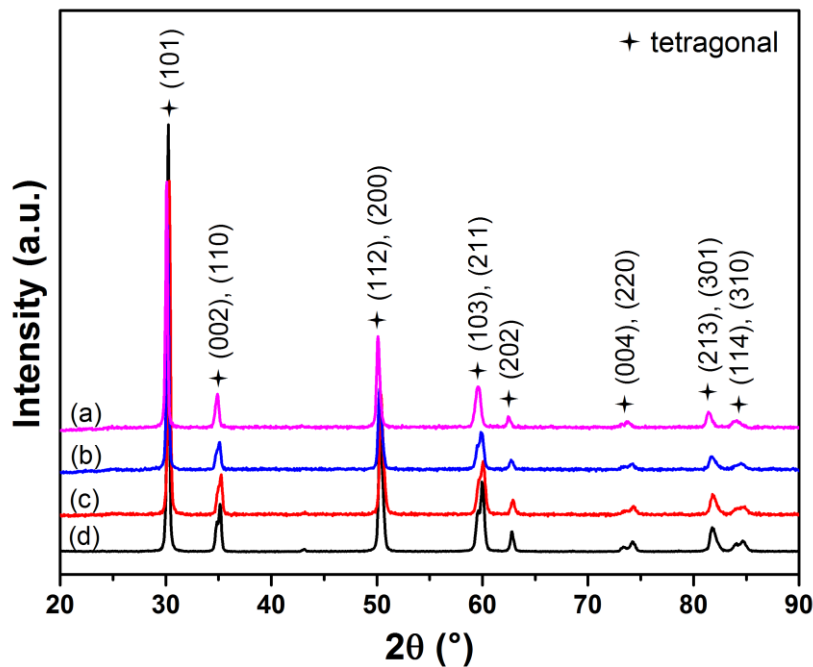
Figure 3. XRD patterns of Dy^{3+}, Al^{3+} and Ce^{4+} doped YSZ calcined at 1200°C for 2 hours: (a) $Dy_{0.03}Ce_{0.05}Y_{0.080}Zr_{0.84}O_{1.945}$; (b) $Dy_{0.03}Al_{0.03}Y_{0.081}Zr_{0.859}O_{1.929}$; (c) $Dy_{0.03}Y_{0.075}Zr_{0.895}O_{1.948}$; and (d) 8YSZ, adapted from [22].
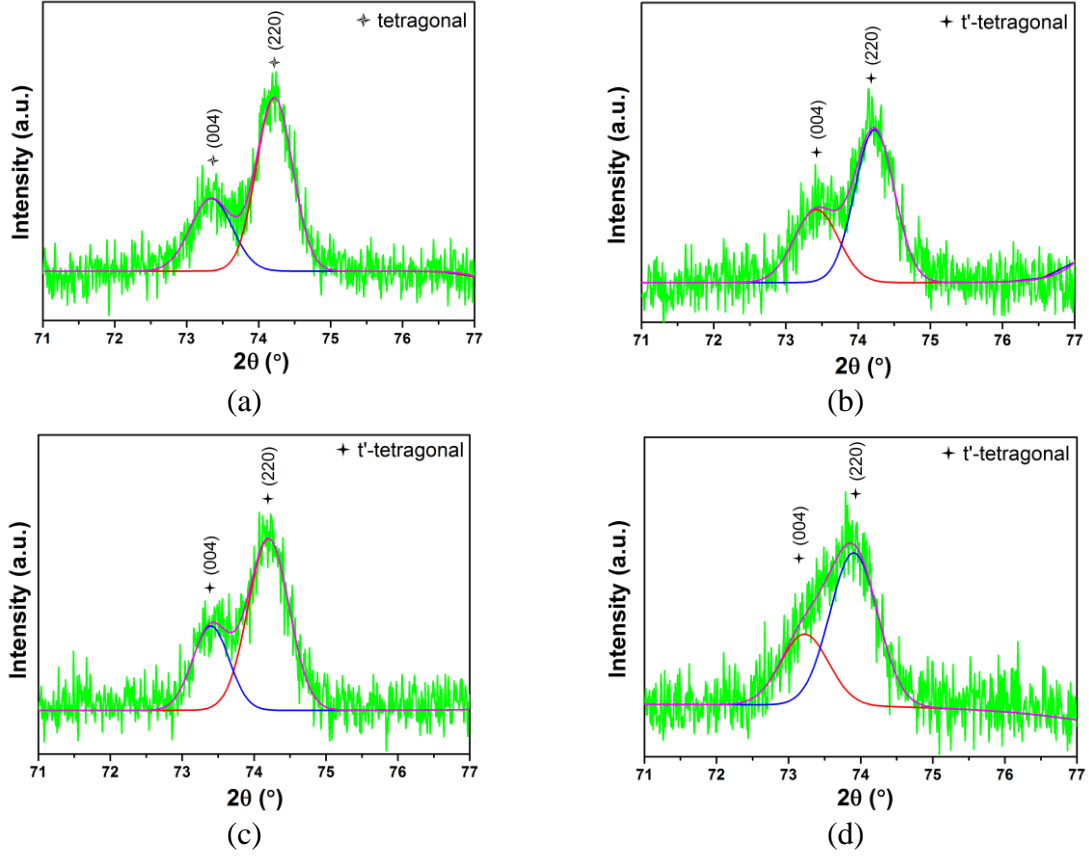
Figure 4. Slow-scan XRD patterns and 2θ-angle differences (δ) between (004) and (220) peaks of: (a) 8YSZ (δ =0.8768°), adapted from [22]; (b) $Dy_{0.03}Y_{0.075}Zr_{0.895}O_{1.948}$ (δ =0.8044°); (c) $Dy_{0.03}Al_{0.03}Y_{0.081}Zr_{0.859}O_{1.929}$ (δ =0.8013°); and (d) $Dy_{0.03}Ce_{0.05}Y_{0.080}Zr_{0.84}O_{1.945}$ (δ =0.6792°).

The crystalline size as estimated by the line broadening using the Scherrer equation shows that the addition of Al^{3+} and Ce^{4+} cations would limit the average crystalline size, as shown in Table 6. Moreover, the grain growth was decreased with the addition of Dy^{3+} and Al^{3+} cations, implying that the sintering resistance of $Dy_{0.03}Ce_{0.05}Y_{0.080}Zr_{0.84}O_{1.945}$ and $Dy_{0.03}Al_{0.03}Y_{0.081}Zr_{0.859}O_{1.929}$ was enhanced, which would be highly desirable for thermal barrier applications.

Temperature	8YSZ	$Dy_{0.03}Y_{0.075}Zr_{0.895}O_{1.948}$	$Dy_{0.03}Al_{0.03}Y_{0.081}Zr_{0.859}O_{1.929}$	$Dy_{0.03}Ce_{0.05}Y_{0.080}Zr_{0.84}O_{1.945}$
950°C	22.51	25.19	21.63	19.74
1200°C	62.03	57.11	54.50	63.61
Difference	39.52	31.92	32.87	43.87

Table 6. Average crystalline size of Dy^{3+}, Al^{3+} and Ce^{4+} doped YSZ at different temperatures (units: nm). 8YSZ data is adapted from [22].

12

Raman analysis was carried out to study the molecular symmetry as presented in Figure 5. Five vibrational modes are observed from 200 cm^{-1} to 800 cm^{-1}, representing the tetragonal structure. For $Dy_{0.03}Al_{0.03}Y_{0.081}Zr_{0.859}O_{1.929}$, 256 cm^{-1} represents the E_g stretching mode; 324 cm^{-1} is the Zr-O B_{1g} bending mode; 465 cm^{-1} indicates the Zr-O stretching E_g mode; 613 cm^{-1} is the symmetric O-Zr-O A_{1g} stretching mode; 638 cm^{-1} represents the asymmetric O-Zr-O E_g stretching mode.[41] This corresponds well with the lattice structure, as determined by XRD, which confirms that the molecular symmetry in Dy^{3+}, Al^{3+} and Ce^{4+} doped YSZ is tetragonal rather than cubic, which is desirable for thermal barrier coatings.
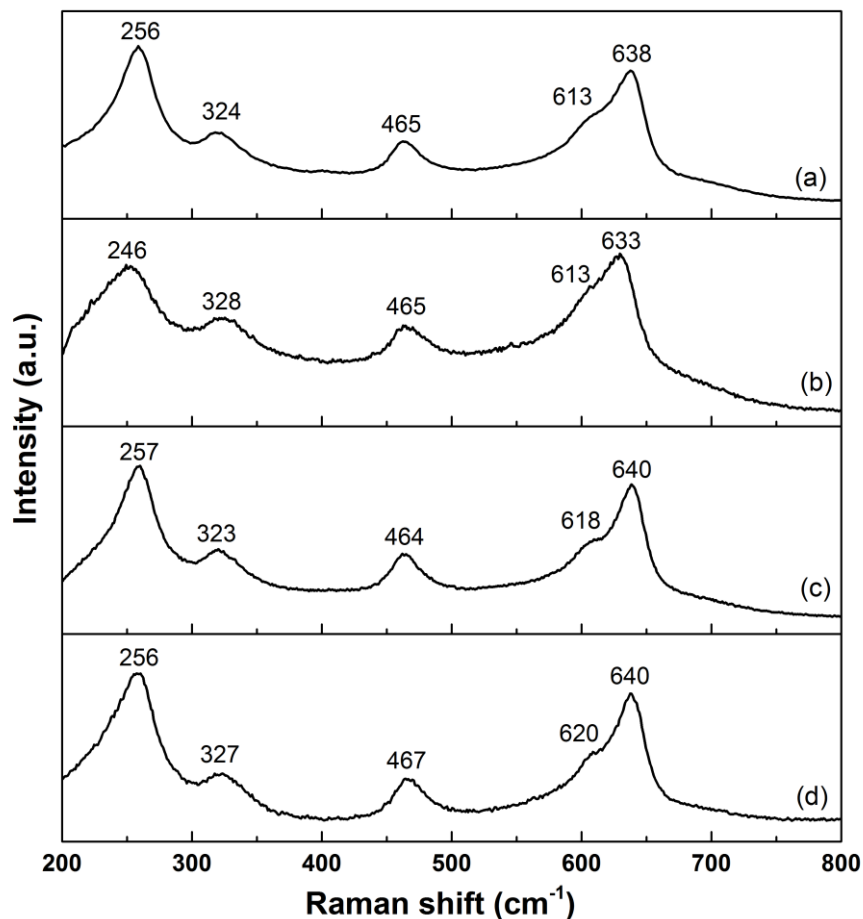

Figure 5. Raman spectra of Dy^{3+}, Al^{3+} and Ce^{4+} doped YSZ: (a) $Dy_{0.03}Al_{0.03}Y_{0.081}Zr_{0.859}O_{1.929}$; (b) $Dy_{0.03}Ce_{0.05}Y_{0.080}Zr_{0.84}O_{1.945}$; (c) $Dy_{0.03}Y_{0.075}Zr_{0.895}O_{1.948}$; and (d) 8YSZ, adapted from [22].

Coefficient of Thermal Expansion

Figure 6 shows the CTE values of Dy^{3+}, Al^{3+} and Ce^{4+} doped YSZ from 300°C to 1000°C. The CTE of each composition was measured twice and the errors were estimated within ±5%. The error bars are not presented because they will result in the difficulty of comparison between different data points at high temperatures. The decrease of CTE above 900°C could be resulted from sintering effect and diffusion of ions.[42,43] The addition of 3 mol% Dy^{3+} cations to ZrO_2 increased the CTE by 9-14%. The increase of the CTE could be due to the lower binding energy of Dy-O (615 $kJ.mol^{-1}$) than that of Zr-O (766.1 $kJ.mol^{-1}$) and the ionic radius of Dy^{3+} (1.03 Å, CN=8) is larger than that of Zr^{4+} (0.84 Å, CN=8).[15] Lower binding energy can enhance the dilation at high temperatures[44, 45]; a larger ionic radius misfit between the doping and host cations leads to a lattice distortion which can weaken the ionic bond.[46-48] Furthermore, the addition of 3 mol% Al^{3+} and 5 mol% Ce^{4+} cations to ZrO_2 increased the CTEs. The binding energy of Al-O (501.9 $kJ.mol^{-1}$) is smaller than that of Zr-O, and the ionic radius of Al^{3+} (0.54 Å, CN=6) is smaller than that of Zr^{4+}. Although the binding energy of Ce-O (790 $kJ.mol^{-1}$) is larger than that of Zr-O, the ionic radius of Ce^{4+} (0.97 Å, CN=8) is larger than that of Zr^{4+} which could bring about the lattice distortion and weaken the ionic bond. The addition of trivalent cations, such as Al^{3+} and Dy^{3+}, could create oxygen vacancies which can weaken the chemical bond and increase the CTE values.[37]
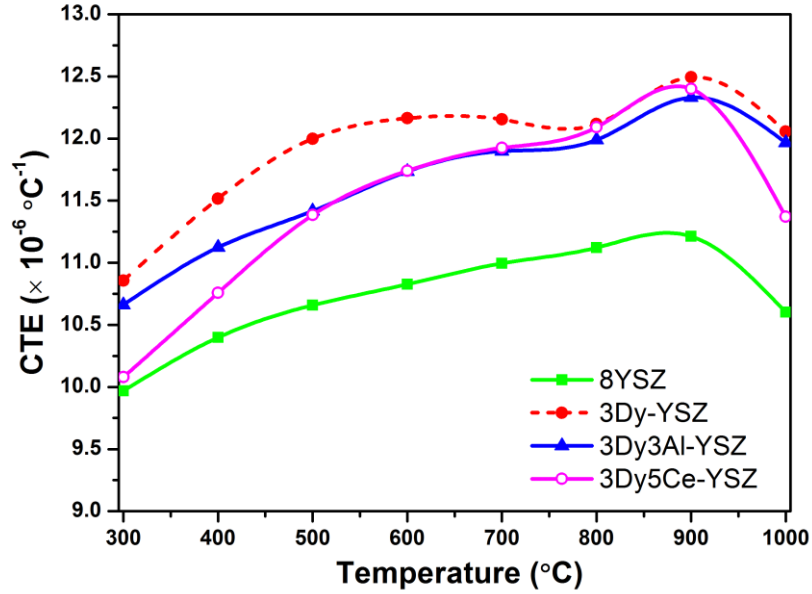
Figure 6. Measured CTEs of Dy^{3+}, Al^{3+} and Ce^{4+} doped YSZ. 8YSZ data is adapted from [22].

Model Validation

The predicted CTE has a deviation of 46-56%, as compared with the measured CTE data (Table 5). These differences could be due to the assumption of the polycrystalline in the bulk sample which has the isotropic CTE over *a*-, *b*- and *c*- axes. Bulk polycrystalline structure tends to contain the imperfections such as grain boundaries, micro-cracks, cation and anion vacancies and porosity which can weaken the ionic bond and increase the CTE value. The simulation unit cell consists of a single crystal that does not contain these imperfections, in part contributing to lower predicted CTE values than the experimental results. Additionally, the interatomic forces for the model are approximate, which means that the predicted CTE will not exactly match that for a perfect crystal lattice. This molecular model of YSZ substituted by trivalent and tetravalent cations has probed the lattice parameters at the atomic scale and predicted the dynamic changes of tetragonality, providing a new and deeper insight into compositional dependent CTE.

15

Conclusions

In this work, MD simulation was used to investigate the impact of doping multiple trivalent and tetravalent cations to 8YSZ on the lattice structure, lattice energy and CTE. Atomic scale insights into synergetic doping effects of trivalent and tetravalent cations with various ionic radius and bonding energy on thermal expansion in ZrO_2 are vital to the materials design and facilitate the selection of suitable multi-cation dopants and their stoichiometries for the development of novel thermal barrier materials, which have also been validated experimentally.

Exploiting the lattice structure and lattice energy of various cations doped YSZ enable us to obtain an in-depth understanding on the anisotropic nature of the tetragonal structure, and discover that doping Dy^{3+}, Al^{3+} and Ce^{4+} would stabilize the tetragonal phase and enhances the thermal expansion properties. The incorporation of Dy^{3+} and Ce^{4+} cations to 8YSZ increased the lattice size, whereas the incorporation of Al^{3+} cation decreased the lattice constant. The lattice energy was decreased due to doping Dy^{3+}, Al^{3+} and Ce^{4+} cations to 8YSZ, while the tetragonal structure has been maintained with the dynamic variation in tetragonality as temperature increases from 295 K to 1873 K. From the experiment, the resistance to grain growth at 1200°C was enhanced by incorporating Dy^{3+} and Al^{3+} cations to 8YSZ, whereas the grain size was reduced due to the addition of Al^{3+} and Ce^{4+}. CTEs of Dy^{3+}, Al^{3+} and Ce^{4+} doped YSZ were increased, as compared with that of 8YSZ, and the doping effects agreed reasonably well with the MD simulation.

Increased resistance to grain growth and enhanced CTEs would allow the thermal expansion mismatch and thermal stress in coatings to be reduced, therefore significantly enhancing the lifetime of thermal barrier materials during the thermal cycling process. Due to the ubiquitous nature of the anisotropic thermal expansion of the tetragonal structure and its importance in high-temperature devices such as solid oxide fuel cells and TBCs, this work gives theoretical CTE values and could accelerate the discovery of novel materials for the technological

applications. This current work and approach can be extended for future studies that focus on comprehensive and systematic simulation of novel materials, for instance, tetragonal, pyrochlore, fluorite and perovskite crystalline system with sophisticated compositions including multiple dopants, for critical applications such as high temperature and extreme environment.

Conflicts of interest

There are no conflicts to declare.

Data availability

All processed data are presented in this paper. The raw data required to reproduce these findings cannot be shared at this time due to technical or time limitations.

References

1. Liang JJ, Wei H, Zhu YL, Sun XF, Hu ZQ, Dargusch MS, et al. Influence of Re on the properties of a NiCoCrAlY coating alloy. J Mater Sci Technol. 2011;27(5):408-14.
2. Padture NP, Gell M, Jordan EH. Thermal barrier coatings for gas-turbine engine applications. Science. 2002;296:280-4.
3. Kilner JA. Ionic conductors: feel the strain. Nat Mater. 2008;7:838-9.
4. Jin H, Breedon M, Tanaka Y, Miura N. Fe-based solid reference electrode utilized in YSZ-based oxygen sensor. ECS Electrochem Lett. 2013;2(1):B1-B3.
5. Cao X, Vassen R, Stoever D. Ceramic materials for thermal barrier coatings. J Eur Ceram Soc. 2004;24(1):1-10.
6. Ballard JD, Davenport JD, Lewis C, Nelson W, Doremus RH, Schader LS. Phase stability of thermal barrier coatings made from 8 wt% yttria stabilized zirconia: a technical note. J Therm Spray Technol. 2003;12(1):34-7.
7. Masó N, West AR. Electronic conductivity in yttria-stabilized zirconia under a small *dc* bias. Chem Mater. 2015;27:1552-8.
8. Xia X, Oldman RJ, Catlow RRA. Oxygen adsorption and dissociation on yttria stabilized zirconia surfaces. J Mater Chem. 2012;22:8594-612.
9. Mercer C, Williams JR, Clarke DR, Evans AG. On a ferroelastic mechanism governing the toughness of metastable tetragonal-prime (t') yttria-stabilized zirconia. Proc R Soc A. 2007;463:1393-408.

10.   Qu Z, Wan C, Pan W. Thermal expansion and defect chemistry of MgO-doped $Sm_2Zr_2O_7$. Chem Mater. 2007;19(20):4913-8.

11.   Yanagida H, Koumoto K, Miyayama M, Yamada H. The Chemistry of Ceramics.1996. 259 p.

12.   Kittel C. Introduction to Solid State Physics. John Wiley & Sons, Inc.; 2005. 675 p.

13.   Qu L, Choy K-L. Thermophysical and thermochemical properties of new thermal barrier materials based on Dy_2O_3-Y_2O_3 co-doped zirconia. Ceram Int. 2014;40(8):11593-9.

14.   Qu L, Choy K-L. An overview of novel tetragonal oxides with enhanced high-temperature capabilities for structural applications. Int J Eng Res Sci. 2016;2(2):14-8.

15.   Lide DR, Haynes WM. CRC handbook of chemistry and physics: a ready-reference book of chemical and physical data. CRC Press, Taylor and Francis Group; 2009.

16.   Wang J, Sun J, Yuan J, Jing Q, Dong S, Liu B, et al. Phase stability, thermo-physical properties and thermal cycling behavior of plasma-sprayed CTZ, CTZ/YSZ thermal barrier coatings. Ceram Int. 2018;44(8):9356-63.

17.   Park SY, Kim HJ, Kim MC, Song HS, Park CG. Microscopic observation of degradation behavior in yttria and ceria stabilized zirconia thermal barrier coatings under hot corrosioin. Surf Coat Technol. 2005;190:357-65.

18.   Lee CH, Kim HK, Choi HS, Ahn HS. Phase transformation and bond coat oxidation behavior of plasma-sprayed zirconia thermal barrier coating. Surf Coat Technol. 2000;124:1-12.

19.   Kirchner HP. Thermal expansion anisotropy of oxides and oxide solid solutions. J Am Ceram Soc. 1969;52(7):379-86.

20.   McGaughey AJH, Kaviany M. Thermal conductivity decomposition and analysis using molecular dynamics simulations. Part I. Lennard-Jones argon. Int J Heat Mass Transf. 2004;47(8-9):1783-98.

21.   Qu L, Choy K-L, Wheatley R. An atomistic-scale study for thermal conductivity and thermochemical compatibility in $(DyY)Zr_2O_7$ combining an experimental approach with theoretical calculation. Sci Rep. 2016;6(21232).

22.   Qu L, Choy K-L, Wheatley R. Theoretical and experimental studies of doping effects on thermodynamic properties of (Dy, Y)-ZrO_2. Acta Mater. 2016;114:7-14.

23.   Schelling PK, Phillpot SR. Mechanism of thermal transport in zirconia and yttria-stabilized zirconia by molecular dynamics simulation. J Am Ceram Soc. 2001;84(12):2997-3007.

24.   Nino JC. Optimization of oxide compounds for advanced inert matrix materials. University of Florida; 2009. Report No.: DE-FC07-O51D14647.

25.   Stanek CR, Minervini L, Grimes RW. Nonstoichiometry in $A_2B_2O_7$ pyrochlores. J Am Ceram Soc. 2002;85(11):2792-8.

26.   Howard MA, Clemens O, Knight KS, Anderson PA, Hafiz S. Synthesis, conductivity and structural aspects of $Nd_3Zr_2Li_{7-3x}Al_xO_{12}$. J Mater Chem A. 2013;1:14013-22.

27.   Li Z-P, Mori T, Zou J, Drennan J. Optimization of ionic conductivity of solid electrolytes through dopant-dependent defect cluster analysis. Phys Chem Chem Phys. 2012;14:8369-75.

28.   Wolf D, Keblinski P, Phillpot SR, Eggebrecht J. Exact method for the simulation of Coulombic systems by spherically truncated, pairwise r^{-1} summation. J Chem Phys. 1999;110(17):8254-82.

29.   Fennell CJ, Gezelter JD. Is the Ewald summation still necessary? Pairwise alternatives to the accepted standard for long-range electrostatics. J Chem Phys. 2006;124(234104):1-12.

30. Andersen HC. Molecular dynamics simulations at constant pressure and/or temperature. J Chem Phys. 1980;72(4):2384-93.

31. Berendsen HJC, Postma JPM, Gunsteren WFv, DiNola A, Haak JR. Molecular dynamics with coupling to an external bath. J Chem Phys. 1984;81(8):3684-90.

32. Ravi V, Firdosy S, Caillat T, Brandon E, Van der Wade K, Maricic L, et al. Thermal expansion studies of selected high-temperature thermoelectric materials. J Electron Mater. 2009;38:1433-42.

33. Wan C, Qu Z, Du A, Pan W. Influence of B site substitutent Ti on the structure and thermophysical properties of $A_2B_2O_7$-type pyrochlore $Gd_2Zr_2O_7$. Acta Mater. 2009;57:4782-9.

34. Romao CP. Anisotropic thermal expansion in flexible materials. Phys Rev B. 2017;96(13):134113.

35. Kirby RK. Thermal expansion of rutile from 100 to 700 °K. J Res Natl Bur Stand A Phys Chem. 1967;71A(5):363-9.

36. Shen F-R, Kuang H, Hu F-X, Wu H, Huang Q-Z, Liang F-X, et al. Utra-low thermal expansion realized in giant negative thermal expansion materials through self-compensation. APL Mater. 2017;5(10):106102.

37. Hayashi H, Saitou T, Maruyama N, Inaba H, Kawamura K, Mori M. Thermal expansion coefficient of yttria stabilized zirconia for various yttria contents. Solid State Ion. 2005;17(5-6):613-9.

38. Schneibel JH, Rawn CJ, Watkins TR, Payzant EA. Thermal expansion anisotropy of ternary molybdenum silicides based on Mo_5Si_3. Phys Rev B. 2002;65(13):134112.

39. Viazzi C, Bonino J-P, Ansart F, Barnabé A. Structural study of metastable tetragonal YSZ powders produced via a sol–gel route. J Alloys Compd. 2008;452(2):377-83.

40. Leib EW, Pasquareli RM, Rosario JJd, Dyachenko PN, Doring S, Puchert A, et al. Yttria-stabilized zirconia microspheres: novel building blocks for high-temperature photonics. J Mater Chem C. 2016;4:62-74.

41. Heiroth S, Frison R, Rupp JLM, Lippert T, Barthazy Meier EJ, Müller Gubler E, et al. Crystallization and grain growth characteristics of yttria-stabilized zirconia thin films grown by pulsed laser deposition. Solid State Ion. 2011;191(1):12-23.

42. Soorie M, Skinner SJ. Thermal expansion and sintering studies of $Nd_{2-x}Ce_xCuO_{4\pm\delta}$ ($0 \leq x \leq 0.20$). J Mater Res. 2006;21(5):1248-54.

43. Ji Y, Kilner JA, Carolan MF. Electrical properties and oxygen diffusion in yttria-stabilised zirconia (YSZ)-$La_{0.8}Sr_{0.2}MnO_{3\pm\delta}$ (LSM) composites. Solid State Ion. 2005;176:937-43.

44. Wu H, Lei X, Zhang J, Yu J, Zhang S. Lattice thermal expansion of the solid solutions $(La_{1-x}Sm_x)_2Ce_2O_7$. Mater Res Bull. 2014;57:320-4.

45. Zhang S, Li H, Zhou S, Pan T. Estimation thermal expansion coefficient from lattice energy for inorganic crystals. Jpn J Appl Phys. 2006;45(11):8801-4.

46. Hayashi H, Kanoh M, Quan CJ, Inaba H, Wang C, Dokiya M, et al. Thermal expansion of Gd-doped ceria and reduced ceria. Solid State Ion. 2000;132(3-4):227-33.

47. Wang J, Bai S, Zhang H, Zhang C. The structure, thermal expansion coefficient and sintering behavior of Nd^{3+}-doped $La_2Zr_2O_7$ for thermal barrier coatings. J Alloys Compd. 2009;476(1-2):89-91.

48. Wang Y-H, Ouyang J-H, Liu Z-G. Influence of dysprosium oxide doping on thermophysical properties of $LaMgAl_{11}O_{19}$ ceramics. Mater Des. 2010;21:3353-7.